Dyes and Pigments 112 (2015) 127–137

Contents lists available at ScienceDirect

Dyes and Pigments

journal homepage: www.elsevier.com/locate/dyepig

Zn(II)-porphyrin dyes with several electron acceptor groups linked by vinyl-fluorene or vinyl-thiophene spacers for dye-sensitized solar cells

Danny Arteaga [a], Robert Cotta [b], Alejandro Ortiz [a], Braulio Insuasty [a, **], Nazario Martin [c], Luis Echegoyen [b, *]

[a] Departamento de Química, Facultad de Ciencias Naturales y Exactas, Universidad del Valle, A.A. 25360 Cali, Colombia
[b] Department of Chemistry, University of Texas at El Paso, 79968-0519 El Paso, TX, United States
[c] Departamento de Química Orgánica, Facultad de Química, Universidad Complutense, 28040 Madrid, Spain

ARTICLE INFO

Article history:
Received 21 April 2014
Received in revised form
19 June 2014
Accepted 24 June 2014
Available online 7 July 2014

Keywords:
Porphyrins
Donor–acceptor systems
Dyes/sensitizers
Solar cells
Molecular wires
Anchoring unit

ABSTRACT

Herein we report the design, synthesis, and characterization of a series of new organic dyes, as well as their application in dye-sensitized nanocrystalline TiO_2 solar cells. In the designed dyes, the diphenylamine Zn(II) porphyrin group plays the role of the core electron donor unit and the cyanoacrylic acid, rhodanine acetic acid, and dicyanorhodanine groups are the acceptors. These electroactive units are linked by either vinyl-fluorene or vinyl-thiophene spacer units. To study the electron distribution and the intramolecular charge transfer the HOMO-LUMO levels of the dyes were calculated by computational methods and experimentally using electrochemical measurements. The DSSCs based on the dyes bearing a cyanoacrylic acid acceptor group showed the best photovoltaic performance with short-circuit photocurrent densities of 12.66 and 13.58 mA/cm^2, open-circuit photovoltages of 0.675 and 0.651 V, and fill factors of 0.628 and 0.441, corresponding to an overall conversion efficiency of 5.56 and 4.13%, respectively, under AM 1.5 irradiation (100 mW/cm^2).

1. Introduction

To capture and use solar energy more cheaply and efficiently the development of new molecules for solar cell technology is of vital importance. With many new types of solar cells being studied and developed, DSSCs have received considerable attention as a cost-effective alternative to conventional inorganic solar cells [1]. DSSCs utilize a dye molecule attached to the surface to enhance a semiconductor's ability to work as a light absorber and charge carrier. A major advantage of DSSCs is the capability to separate the two functions, facilitating the production of the device. Other advantages with DSSCs are flexibility, reduced energy payback time, and relatively high performance at diffuse light conditions [2].

The sensitizers for DSSCs can be grouped into two broad areas: functional ruthenium (II)–polypyridyl complexes [3] and metal-free, organic donor–acceptor (D–A) dyes. Generally, the DSSCs with ruthenium (II) complexes as sensitizers have proven to be the best performers; however, the price of ruthenium makes these sensitizers too expensive for mass production. On the other hand, pure organic dyes can be prepared rather inexpensively following established design strategies.

Organic dyes tend to have many advantages over these metal dyes, such as higher absorption coefficients and easy control of redox potentials of the highest occupied molecular orbital (HOMO) and lowest unoccupied molecular orbital (LUMO) levels [4]. These dyes can be classified into several types of systems such as donor–acceptor (D–A), donor–bridge–acceptor (D–B–A) and acceptor–bridge–acceptor (A–B–A) systems that have applications as electroactive and photoactive materials in the field of molecular electronics, mainly photovoltaic technologies [5].

Large π-aromatic molecules such as porphyrins [6], phthalocyanines [7], anthocyanins [8], ferrocene [9], π-extended tetrathiafulvalene (exTTF) [10], and triphenylamine [11] are important classes of donors. These are usually functionalized with various electron acceptor anchoring groups [12]. such as cyanoacrylic acid and its analogs [13], rhodanines [14], and pyridines [15] as the active layers in DSSCs because they tend to be highly efficient. To link these photoactive units, a π-bridge is typically used to facilitate intramolecular charge transfer from the donor to the acceptor. Conjugated groups such as carbazole [16], fluorene [17],

* Corresponding author. Tel.: +1 9157477573.
** Corresponding author. Fax: +57 2 3393248.
E-mail addresses: Braulio.insuasty@correounivalle.edu.co (B. Insuasty), Nazmar@quim.ucm.es (N. Martin), Echegoyen@utep.edu (L. Echegoyen).

http://dx.doi.org/10.1016/j.dyepig.2014.06.028
0143-7208/

spirobifluorene [18], oligothiophene [19], and dithienothiophene [20], have been used as π-bridges between the electron donor and acceptor to tune the absorption parameters and photovoltaic performance.

Based on these findings and previous work on functionalized-porphyrin dyes for DSSCs by Grätzel and co-workers [6b], we have designed and synthesized new push–pull systems containing a diphenylamine-Zn(II)-porphyrin derivative as the electron donor group, a vinylfluorene or vinylthiophene as the π-bridge, and cyanoacrylic acid, rhodanine acetic acid, or dicyanorhodanine as the anchoring acceptors groups. Herein, we report the synthesis and characterization as well as the optical, electrochemical, and photovoltaic properties of six new push–pull organic dyes (**5a**–**c** and **7a**–**c**), shown in Fig. 1, and their application as potential sensitizers for the fabrication of photovoltaic devices.

2. Results and discussion

2.1. Synthesis of dyes *5a–c* and *7a–c*

The preparation of the push–pull systems was carried out using multiple reactions, including the Ullman and Heck cross-coupling reactions and the Knoevenagel condensation, see Fig. 1.

The general procedure used for the preparation of the dyes containing a diphenylamine-based Zn(II)-porphyrin donor, vinyl-fluorene/vinyl-thiophene π-bridges, and cyanoacrylic acid, 4-oxo-2-thioxo-3-thiazolidinylacetic acid or 2-(1,1-dicyanomethylene)-1,3-thiazol-4-one as acceptor anchoring groups is depicted in Fig. 1. The starting Zn(II) porphyrin 1 was prepared using literature procedures [6a,6b]. The Zn(II) porphyrin derivative was functionalized with diphenylamine by an Ullman reaction to obtain the functionalized Zn(II) porphyrin 2 [6a]. Zn(II) porphyrin **3** was prepared by a bromination reaction with *N*-bromosuccinimide (NBS). The photoactive dyads **4** and **6** were obtained by a palladium-catalyzed Heck cross-coupling reaction using anhydrous dimethylformamide (DMF) as the solvent. Dyads **4** and **6** were later converted to the desired dyes **5a**–**c** and **7a**–**c** in good yields by different Knoevenagel condensations using cyanoacetic acid, 4-oxo-2-thioxo-3-thiazolidinylacetic acid, or 2-(1,1-dicyanomethylene)-1,3-thiazol-4-one in the presence of the appropriate catalysts, either ammonium acetate ($AcNH_4$) or piperidine and using acetic acid (AcOH) or ethanol (EtOH) as the solvents, respectively. The 2-(1,1-dicyanomethylene)-1,3-thiazol-4-one was obtained using a previously reported synthesis [21].

The new dyes were thoroughly characterized by analytical measurements and spectroscopic techniques, ^{1}H-NMR and ^{13}C-NMR, and matrix-assisted laser desorption/ionization time of flight mass spectroscopy (MALDI-TOF MS) and the spectral data correlated with the structures, (see ESI).

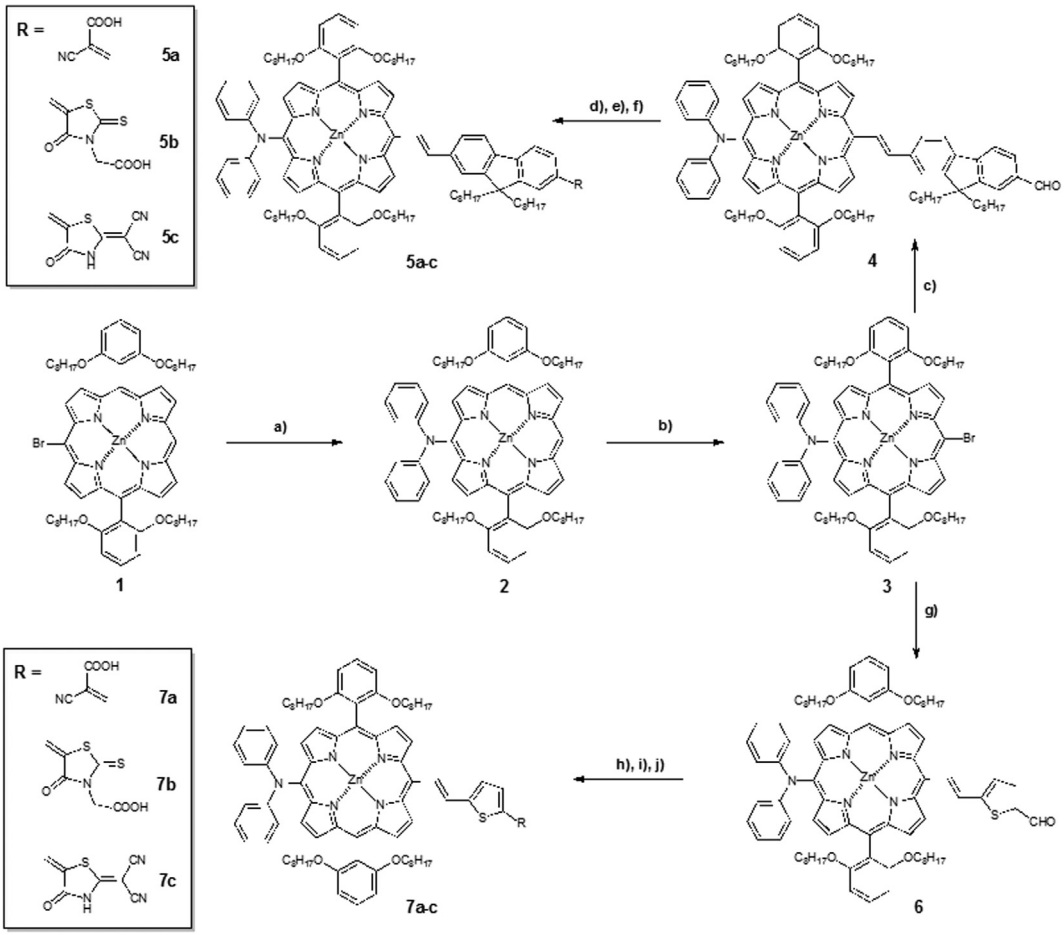

Fig. 1. Synthetic strategies for the preparation of the novel dyes **5a**–**c** and **7a**–**c**. Reagents and conditions (a) Diphenylamine, 60% NaH, DPEPhos, $Pd(OAc)_2$, THF, 70 °C (**2**, 70%); (b) NBS, DCM, 0 °C, (**3**, 87%); (c) 9,9-dioctyl-7-vinyl-9*H*-fluorene-2-carbaldehyde, $Pd(OAc)_2$, TBAB, K_2CO_3, DMF, 110 °C (**4**, 81%); (d) **4**, cyanoacetic acid, piperidine, EtOH/DCM, reflux (**5a**, 72%); (e) **4**, 4-oxo-2-thioxo-3-thiazolidinylacetic acid, $AcNH_4$, AcOH, reflux (**5b**, 70%); (f) 4, 2-(1,1-dicyanomethylene)-1,3-thiazol-4-one, piperidine, EtOH/DCM (**5c**, 75%); (g) 5-vinylthiophene-2-carbaldehyde, $Pd(OAc)_2$, TBAB, K_2CO_3, DMF, 110 °C (**6**, 64%); (h) **6**, cyanoacetic acid, piperidine, EtOH/DCM, reflux (**7a**, 70%); (i) 6, 4-oxo-2-thioxo-3-thiazolidinylacetic acid, $AcNH_4$, AcOH, reflux (**7b**, 65%); (j) 6, 2-(1,1-dicyanomethylene)-1,3-thiazol-4-one, piperidine, EtOH/DCM, reflux (**7c**, 68%).

2.2. Absorption and emission properties

The absorption and emission spectra were recorded in tetrahydrofuran (THF) and the results are reported in Table 1 and Fig. 2. The absorption spectra of dyes **5a**–**c** and **7a**–**c** and reference compound **3** are shown in Fig. 2a. The dyes exhibit strong Soret bands and weak *Q* bands typical of porphyrin absorption. The Soret bands (absorption maxima) contribute to the transitions appearing in the 439–454 nm range and the *Q* bands observed between 574 and 664 nm are overlapped with the intramolecular charge transfer bands (ICT) between the porphyrin core donor unit and the electron–acceptors. Also observed is an additional band around 350 nm that corresponds to the $\pi \rightarrow \pi^*$ electronic transition. When comparing the π-bridges, the thiophene containing dyes **7a**–**c** exhibit red-shifted absorption spectra when compared to the corresponding fluorene derivatives **5a**–**c**. This is attributed to the enhanced electronic coupling between the donor and acceptor entities in **7a**–**c** due to the thiophene unit, which provides better conjugation than the fluorene moiety and lowers the energy of the charge transfer for conjugated dipolar molecules. Fig. 2b shows the normalized emission and absorption spectra of dyes **5a**–**c** and **7a**–**c** in THF solutions.

The excitation wavelength for the emission spectra was 450 nm and the maxima were observed in the range of 649–698 nm. As seen in the absorption spectra, the emission spectra were also red-shifted because of the difference between the thiophene and fluorene derivatives. The relative fluorescence quantum yields (ϕ_F) of **5a**–**c** and **7a**–**c** are summarized in Table 1 and were calculated using Equation (1) [22] with **3** as the standard, where F and F^{Std} are the respective areas of the fluorescence plots of each dye **5a**–**c**, **7a**–**c** and the standard. A and A^{Std} are the maximum absorbance intensities of the each sample and standard; I and I^{Std} are the relative intensities of the exciting light, and n^2 and n^2_{Std} are the refractive indices of the solvent used for the measurements.

$$\phi_F = \phi_F^{Std} \frac{FA^{Std} In^2}{F^{Std} AI^{Std} n^2_{Std}} \quad (1)$$

The quantum yield values of **5a**–**c** and **7a**–**c** are found in the range of 2.9×10^{-2} to 9.4×10^{-2} relative to that of the reference, **3,** which was assigned the value of 1 ($\phi_F = 1$) for comparison. Relative to the photophysical properties and the quantum yield assigned to this porphyrin reference, the lower ϕ_F values of sensitizers **5a**–**c** and **7a**–**c** are due to the presence of the electron acceptor anchoring groups, which provides insight into the excited state deactivation pathways.

Table 1
Electronic absorption and emission data including quantum yields for dyes **5a**–**c** and **7a**–**c**.

Dye	Absorption[a]	Emission[b]	ϕ_F[c]
	λ_{max} [nm] (ε, [10^4 $Lmol^{-1}$ cm^{-1}])	λ_{max} [nm]	
5a	451 (9.70), 575 (1.10), 637 (1.70)	649	6.8×10^{-2}
5b	449 (9.30), 575 (1.00), 636 (1.60)	661	9.4×10^{-2}
5c	454 (9.00), 575 (0.90), 634 (1.50)	657	6.6×10^{-2}
7a	452 (9.10), 574 (1.20), 652 (2.30)	679	3.7×10^{-2}
7b	439 (7.50), 577 (1.20), 664 (2.20)	667	8.8×10^{-2}
7c	454 (6.90), 576 (1.00), 652 (1.90)	698	2.9×10^{-2}

[a] Absorption spectra of dyes measured in THF at 1×10^{-5} M.
[b] The excitation wavelength for the emission was ~450 nm.
[c] Quantum yields relative to the diphenylamine-porphyrin (**3**) used as the standard reference ($\phi_F = 1$).

2.3. Electrochemical properties

The electrochemical measurements were recorded in dry dichloromethane (DCM) containing 0.1 M tetrabutylammonium hexafluorophosphate ($TBAPF_6$) as the supporting electrolyte. These results are displayed in Fig. 3, and the corresponding data are summarized in Table 2. The HOMO and LUMO energy levels were calculated from solution-based measurements to determine the band-gap alignment in relation to the conduction band (CB) of TiO_2 and the energy level of the electrolyte (I^{3-}/I^-) The parameters were determined by recording the redox properties of the dyes using cyclic voltammetry (CV) at room temperature. The electrochemical properties are summarized in Table 2 and the cyclic voltammograms recorded for the dyes are shown in Fig. 3. All dyes displayed reversible oxidation processes at potentials higher than that observed for the internal ferrocene/ferrocenium couple, attributed to the removal of electrons from the Zn(II) porphyrin unit. The oxidation potential of all dyes were determined from the $E_{1/2}$ of the oxidation relative to the internal ferrocene standard. The oxidation potential vs. Normal Hydrogen Electrode (NHE) known as E_{ox} corresponds to the HOMO.

As seen in Table 1, both the HOMO and LUMO levels of these dyes are suitable for effective sensitization. The HOMO energy level of the dyes have potentials ranging from 0.73 to 0.76 V vs. NHE, which are higher than that of the I^{3-}/I^- redox couple ($\approx$0.40 V vs. NHE) [1], indicating an effective regeneration of the oxidized state. The LUMO energy levels of the dyes range from −1.07 to −1.20 V vs. NHE, lower than the energy level of the CB of TiO_2 ($\approx$−0.5 V vs. NHE) [23], with the E_{gap} ranging from 0.57 to 0.70 V. Assuming that an energy gap of 0.2 eV is necessary for efficient electron injection, these driving forces are sufficient for effective electron injection into the TiO_2 CB (Fig. 4).

2.4. Theoretical calculations

In order to understand the optical and electrochemical properties of dyes **5a**–**c** and **7a**–**c** we modeled the electronic structures by gas-phase theoretical calculations. All structures were optimized using the GAUSSIAN-09 package at the density functional theory (DFT) level [24]. M06 was the meta-hybrid function employed, including the last dispersion approximation by Truhlar [25]. The basis set chosen for all the atoms was Pople's 6-31G**.

Conformational changes were also analyzed and no energy variation were found. It is worth noting that the connection between the donor and acceptor fragments through the π-conjugated bridge did not influence the torsional angle, so a high degree of conjugation and strong electronic coupling exists between the two fragments.

Deeper analyses of the orbital shape showed the clear donor–acceptor behavior. The LUMO was well distributed around the π-bridge and acceptor units in all cases (Fig. 5). The HOMO was mainly localized on the porphyrin core and showed good overlap with the π-orbitals of the benzyl groups, which provide electronic coupling to the aromatic chain. The orbitals of the metal atom contributed highly to an increase in the electronic distribution of the HOMO throughout the entire porphyrin, where the metal atom also exhibited back bonding to the π-conjugated system.

As shown in Fig. 5, the optimized geometries and shapes of the molecular orbitals of the sensitizers show very similar charge transfer distribution, i.e., the HOMO and the LUMO of each system had very similar shapes. This suggests that the LUMO levels of all dyes should be capable of injecting electrons into the CB of the TiO_2. Table 3 summarizes the frontier orbital energies of the

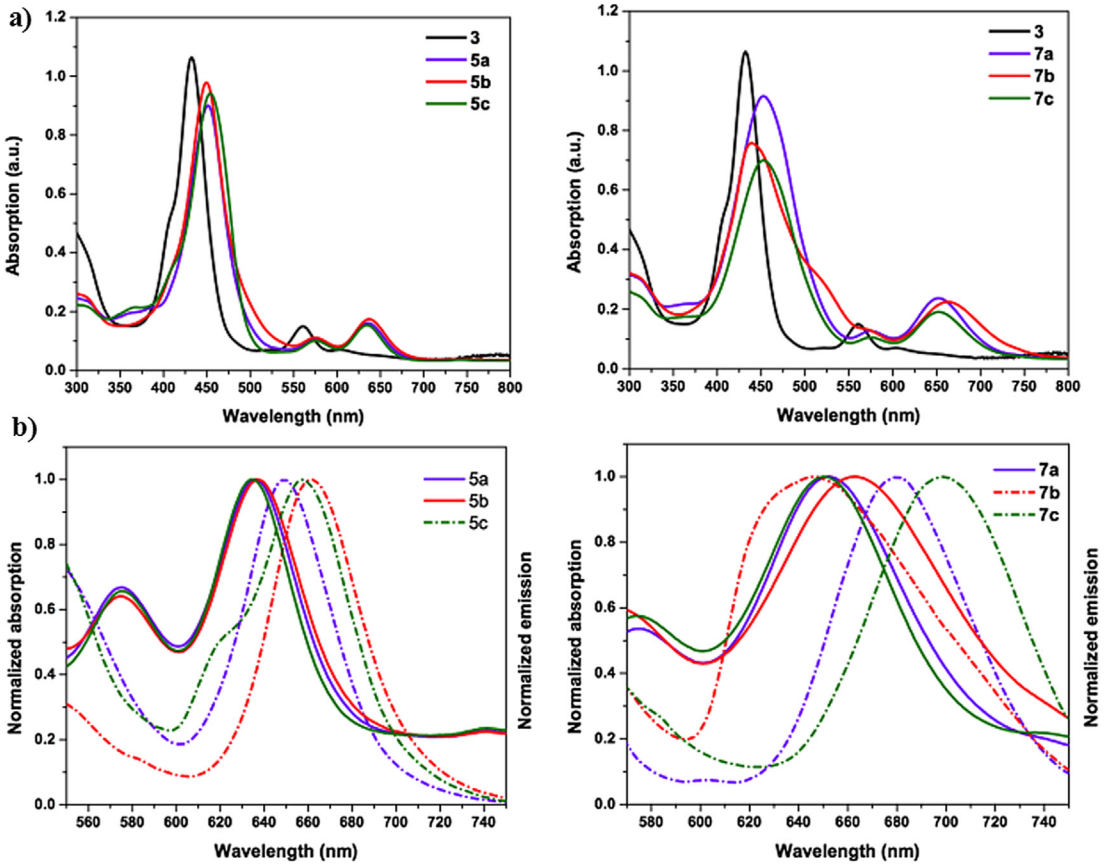

Fig. 2. (a) UV–Visible absorption spectra of the dyes **5a**–**c** and **7a**–**c** in THF solutions, (b) Normalized absorption of Q bands (solid lines) and emission (dashed lines) spectra of the dyes **5a**–**c** and **7a**–**c** in THF.

computed structures, as well as the LUMO+1 and HOMO−1. In general, the orbital's energies are very consistent, with minimal differences in energy on the order of meV. Both the HOMO and LUMO energies are almost unperturbed when compared with those of the independent porphyrin and acceptor units respectively.

2.5. Solar cell performance

The photovoltaic curves of the DSSCs based on dyes **5a**–**c** and **7a**–**c** are shown in Fig. 6 and the photovoltaic performance parameters are given in Table 4 with parameters for the N719 standard provided for comparison. Dye performance efficiencies were

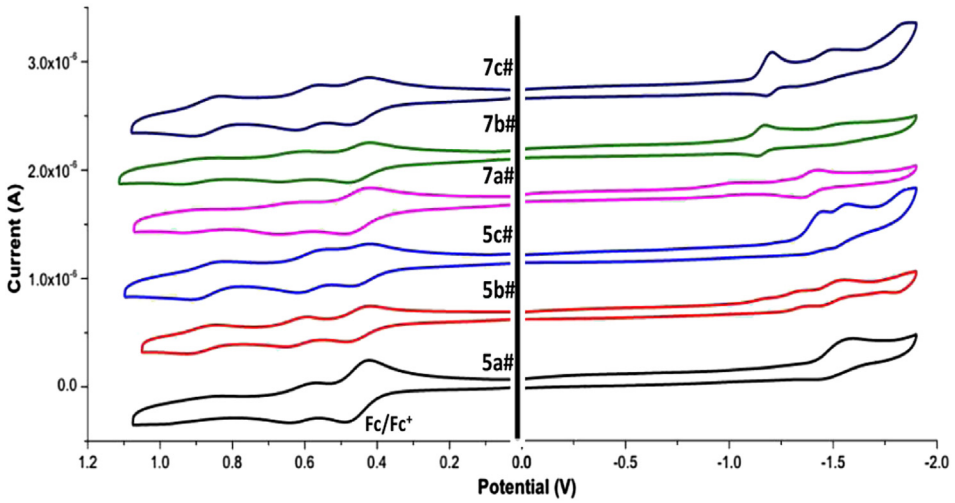

Fig. 3. Cyclic voltammograms for dyes **5a**–**c** and **7a**–**c** in DCM at room temperature, oxidative scans between 0 and 1.05 V; reductive scans between 0 and −2.05 V.

Table 2
Electrochemical properties of the dyes **5a**–**c** and **7a**–**c**.

Dye	E_{ox}/V[a] (*vs.* NHE)	E_{0-0}/eV[b]	$E_{ox} - E_{0-0}$/V[c] (*vs.* NHE)	E_{gap}/V[d]
5a	0.73	1.93	−1.20	0.70
5b	0.77	1.91	−1.14	0.64
5c	0.75	1.92	−1.17	0.67
7a	0.79	1.86	−1.07	0.57
7b	0.77	1.89	−1.12	0.62
7c	0.76	1.84	−1.08	0.58

[a] The E_{ox} referenced to Fc/Fc^+ couple was converted to the NHE reference scale: $E_{ox} = E_{1/2} + 0.63$ V.
[b] E_{0-0} values were calculated from the intersection of the normalized absorption and the emission spectra (λ_{int}): $E_{0-0} = 1240/\lambda_{int}$.
[c] The E_{red} *vs.* NHE were calculated using the expression $E_{ox}-E_{0-0}$.
[d] E_{gap} is the energy gap between the E_{red} of dye and the CB level of TiO_2 (−0.5 V *vs.* NHE).

7b < **5c** < **7c** < **5b** < **7a** < **5a**. The DSSCs based on **5a** and **7a** exhibited the best photovoltaic characteristics, with fairly high power conversion efficiencies.

Open-circuit voltages and short-circuit currents for DSSCs are known to depend on several factors, and some of the most important are the degree of delocalization of the dye's LUMO on the molecule and on the acceptor anchor group, the tilt angle of the dye molecule relative to the TiO_2 surface, the accessibility of the electrolyte to the semiconductor electrode surface, and the dye loading amounts. When looking at the results in Table 4, the most striking and consistent observation is the higher short circuit currents observed for **5a** and **7a** (12.66 and 13.58 mA/cm^2, respectively), which are similar and comparable to the current measured for the reference compound under similar conditions (13.96 mA/cm^2 for N719). Higher photocurrents have been observed for dyes possessing the cyanoacrylic acid anchoring group (**5a** and **7a**) because they lead to highly efficient electron injection into the semiconductor, more so than the rhodanine anchor (**5b** and **7b**), and also because they orient the corresponding dyes in a perpendicular arrangement relative to the TiO_2 surface [26]. The perpendicular orientation presumably inhibits the inner-path recombination between the semiconducting electrode and the dye cation immediately following electron injection. For the rhodanine-anchored dyes (**5b** and **7b**), the orientation is considerably tilted relative to the TiO_2 surface, a situation that enhances the non-productive, inner-path recombination of the injected electrons. We thus believe that one of the main reasons for the observed results is the optimal

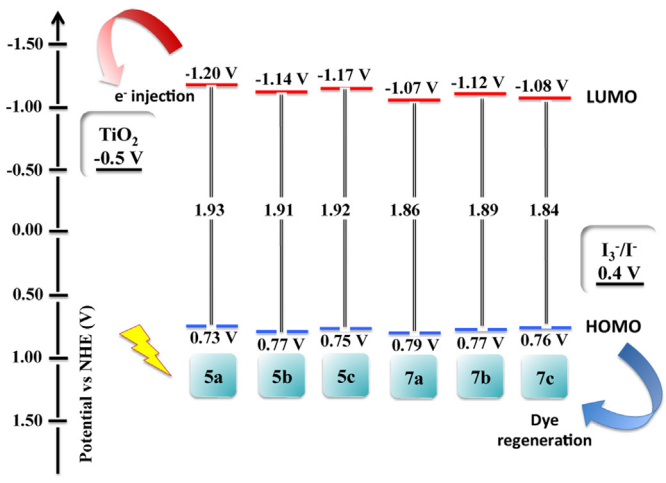

Fig. 4. Energy levels of the dyes **5a**–**c** and **7a**–**c** and of the materials used for the fabrication the DSSC devices.

properties of the cyanoacrylic acid anchoring group, which provides favorable electron injection and appropriate dye orientation on the surface, while also minimizing a high LUMO contribution at the anchor, that would otherwise favor inner-path recombination [26]. The dicyano rhodanine anchor is a very good acceptor that possesses similar electron injecting abilities as its cyanoacrylic acid counterpart and should also lead to a vertical dye orientation, producing similar photocurrents [14c]. Based on these factors, it would thus be predicted to be a very effective anchoring group as well, but the LUMOs show that much of the electron density is localized on these dicyano rhodanines, a situation that is known to lead to efficient inner-path recombination, yielding decreased photoconversion efficiencies. While the results in Table 4 clearly show that this anchoring group is better than rhodanine in the **7b**–**7c** series, the reverse is true for the **5b**–**5c** series, indicating that the linker must be playing an important role as well.

As expected, the more delocalized and alkyl chain protected vinyl-fluorene groups are more effective than the corresponding vinyl-thiophenes (efficiencies: **5a** > **7a** and **5b** > **7b**), especially when considering the dye loading differences. Dyes **5a** and **7a** have comparable loading, but the loading is significantly higher for **7b** than **5b**. Based on this, **5c** would have been predicted to be more efficient than **7c**, which is not the case. Perhaps this is due to the substantial dye loading difference (see Table 4) or a subtle interplay between effective linker delocalization and the acceptor anchoring group. The extremely low fill factor observed for **7a** remains unexplained at the present time. All of these factors affect the open-circuit voltages and are known to lead to a decreased TiO_2 conduction band, which can ultimately lead to lower V_{oc} values. This decrease is usually observed when negative dipoles are created at the dye:TiO_2 interface due to poor electronic structuring of the dye [26].

In summary, the preferred anchor of the three studied here is cyanoacrylic acid because of its favorable electronic properties and appropriate surface orientation of the dyes. Also, since it is not as strong of an electron acceptor as dicyano rhodanine, it does not favor the unproductive inner-path recombination. It is also concluded that the preferred linker is the vinyl-fluorene, likely due to its extended π structure and its alkyl chain substitution that inhibits the detrimental outer-path recombination between the electrolyte and the semiconductor after electron injection.

The external quantum efficiencies (EQE) of all dyes are shown in Fig. 7 and these results correlate well with the observed photoconversion efficiencies in Table 4, with **5a** and **7a** also showing the highest EQE percentages. The large peak observed at 350 nm corresponds to the TiO_2 absorption, while the other peaks correspond to the absorption spectra of the dyes. The *Q* to Soret band intensity ratio changes due to the anchoring of the dye onto the TiO_2 surface, a phenomenon that is well documented [6b]. Dye loading of the cells greatly affects the observed EQE data and band intensities as can be seen from the comparison of dyes **5a** to **5c** and **7a** to **7c**.

3. Conclusions

In summary, we have prepared six new organic dyes with a D-π-A (Donor-π bridge-acceptor) structure for DSSC applications. These new dyes contain a diphenylamine-Zn(II)porphyrin donor; a cyanoacrylic acid, rhodanine acetic acid, or dicyanorhodanine as acceptors; and vinylfluorene or vinylthiophene as π-linkers. The cyanoacrylic acid derivatives are effective as sensitizers in DSSCs based on nanocrystalline TiO_2. The dyes that exhibited the best performance were **5a** and **7a**, with corresponding photoconversion efficiencies of 5.56 and 4.13%, respectively. The devices exhibit an open-circuit voltage (V_{oc}) of 0.675 and 0.651 V, a moderate circuit

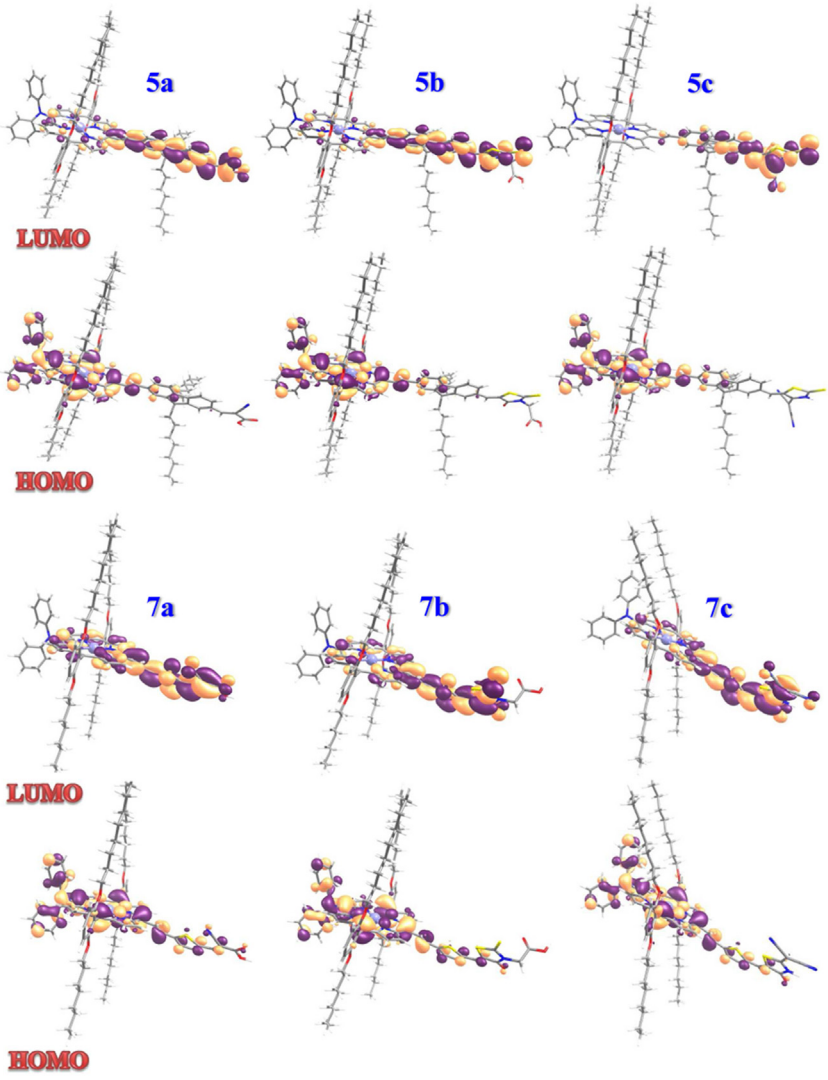

Fig. 5. Frontier orbitals of the new push–pull dyes **5a–c** and **7a–c** optimized at the B3LYP/6-31G** level.

photocurrent density (J_{sc}) of 12.66 and 13.58 mA/cm^2 and a fill factor (ff) of 0.628 and 0.441.

4. Experimental

4.1. Materials and equipments

All reagents and solvents were obtained from commercial sources and used without further purification. $TBAPF_6$ was recrystallized twice from absolute EtOH and further dried for one day under vacuum before use. NMR spectra were recorded using a JEOL 600 MHz NMR spectrometer. MALDI–TOF spectra were obtained using a Bruker MicroFlex LRF mass spectrometer. The UV–Vis spectra were recorded using a Cary 5000 UV–Vis–NIR spectrophotometer. The electrochemical measurements were performed using a CH Instruments electrochemical system in anhydrous and degassed DCM containing 0.1 M $TBAPF_6$ as the supporting electrolyte. The elemental analysis of each compound was obtained using a Thermo Finnigan Flash EA 1112. CHN (STIUJA) elemental analyzer. Melting points were determined on a Stuart SMP10 apparatus.

Table 3
Computed energy levels of the frontier orbitals of all the calculated structures dyes **5a–c** and **7a–c**.[a]

Dye	5a	5b	5c	7a	7b	7c
LUMO+1	−2.033	−2.048	−2.272	−1.969	−1.993	−2.167
LUMO	−2.448	−2.424	−3.622	−2.632	−2.607	−2.873
HOMO	−4.937	−4.910	−5.039	−5.013	−4.978	−5.112
HOMO−1	−5.221	−5.198	−5.315	−5.291	−5.274	−5.384

[a] Energies are reported in eV.

4.2. Synthesis

All reactions were carried out under argon with the use of standard inert atmosphere and Schlenk techniques. The solvents were dried by standard procedures such as sodium/benzophenone and/or calcium hydride (CaH_2), then freshly distilled before use.

4.2.1. Compound *1*

Compound **1** was synthesized by following a literature procedure [6a,6b]. Purple solid, mp = 129 °C. ^{1}H NMR (600 MHz, $CDCl_3$) δ_H 0.28–0.56 (m, 44H), 0.72–0.79 (m, 8H), 0.86–0.93 (m, 8H), 3.81 (t, J = 6.4 Hz, 8H), 6.99 (d, J = 8.3 Hz, 4H), 7.68 (t, J = 8.3 Hz, 2H), 8.95 (d, J = 4.6 Hz, 2H), 8.97 (d, J = 4.6 Hz, 2H), 9.23 (d, J = 3.7 Hz, 2H),

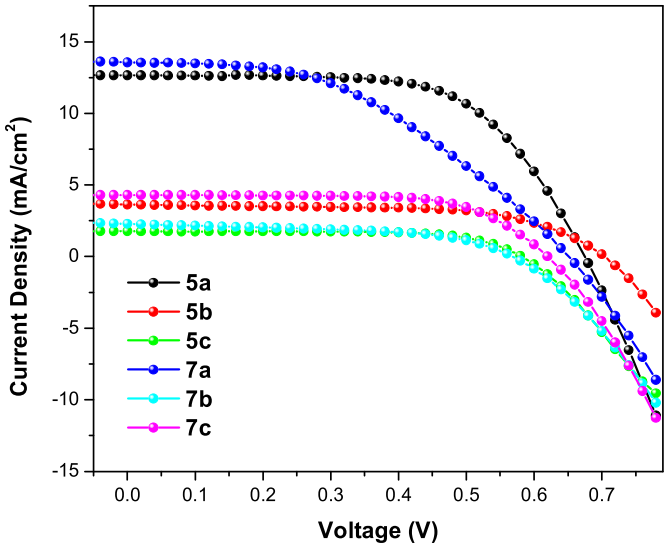

Fig. 6. PV curves of devices based on **5a–c** and **7a–c** dyes under the AM 1.5 solar simulation.

9.67 (d, $J = 4.6$ Hz, 2H), 10.10 (s, 1H) ppm; ^{13}C NMR (151 MHz, $CDCl_3$) δ_C 13.8, 22.2, 25.2, 28.4, 28.5, 28.6, 31.3, 68.8, 103.7, 105.4, 105.5, 113.7, 121.2, 129.9, 131.6, 132.2, 132.3, 132.4, 148.9, 150.1, 151.2, 160.1 ppm; FT-IR (KBr) υ = 3088, 2950, 2923, 2851, 1587, 1492, 1458, 1437, 1374, 1264, 1240, cm^{-1}; MS (MALDI-TOF): *m/z* 1114.243. Anal. Calcd. for $C_{64}H_{83}BrN_4O_4Zn$: C, 68.88; H, 7.44; N, 5.02. Found: C, 69.07; H, 7.53; N, 5.05.

4.2.2. Compound **2**

A solution of porphyrin **1** (600 mg, 0.54 mmol), diphenylamine (363.3 mg, 2.16 mmol), 60% sodium hydride (NaH) (257.4 mg, 10.74 mmol), (oxydi-2,1-phenylene)bis(diphenylphosphine) (DPE-Phos) (231.3 mg, 0.42 mmol) and palladium acetate ($Pd(OAc)_2$) (48.3 mg, 0.22 mmol) in dry THF (50 mL) was heated at 70 °C under an inert atmosphere for 12 h. The solvent was removed under vacuum. The crude was purified by column chromatography (silica gel) using $CHCl_3$:hexanes (1:1) as the eluant to give the product (454 mg, 70%) as a purple solid, mp = 125 °C. ^{1}H NMR (600 MHz, $CDCl_3$) δ_H 0.38–0.64 (m, 44H), 0.76–0.81 (m, 8H), 0.91–0.96 (m, 8H), 3.81 (t, $J = 6.4$ Hz, 8H), 6.80 (t, $J = 7.3$ Hz, 2H), 6.96 (d, $J = 9.2$ Hz, 4H), 7.11 (t, $J = 7.8$ Hz, 4H), 7.32 (d, $J = 7.3$ Hz, 4H), 7.65 (t, $J = 8.3$ Hz, 2H), 8.81 (d, $J = 4.6$ Hz, 2H), 8.94 (d, $J = 4.6$ Hz, 2H), 9.22 (d, $J = 3.7$ Hz, 2H), 9.26 (d, $J = 3.7$ Hz, 2H), 10.03 (s, 1H) ppm; ^{13}C NMR (151 MHz, $CDCl_3$) δ_C 13.9, 21.3, 22.4, 24.7, 25.2, 27.7, 28.5, 28.6, 28.7, 29.6, 29.8, 31.4, 45.2, 63.7, 68.6, 77.8, 105.3, 105.5, 113.0, 120.4, 121.1, 122.1, 128.9, 129.8, 130.1, 131.4, 131.9, 132.4, 149.6, 150.0, 151.0, 151.7, 152.6, 160.0, 172.7 ppm; FT-IR (KBr) υ = 3057, 2950, 2923, 2851, 1588, 1490, 1458, 1435, 1264, 1240 cm^{-1}; MS (MALDI-TOF): *m/z* 1203.221. Anal. Calcd. for $C_{76}H_{93}N_5O_4Zn$: C, 75.75; H, 7.72; N, 5.81. Found: C, 75.66; H, 7.81; N, 5.70.

Table 4
Performance parameters of the DSSC devices using dye **5a–c** and **7a–c** against the N719 standard. Approximate areas were 0.25 cm^2 and measurements were conducted at approximately 100 mW/cm^2.

Dye	J_{SC} (mA/cm^2)	V_{OC} (V)	*ff*	η (%)	Dye load (mol/cm^2)
5a	12.66	0.675	0.628	5.56	1.83×10^{-7}
5b	4.21	0.691	0.666	2.32	4.42×10^{-8}
5c	1.77	0.581	0.694	0.73	5.72×10^{-9}
7a	13.58	0.651	0.441	4.13	2.87×10^{-7}
7b	2.28	0.589	0.531	0.71	1.07×10^{-7}
7c	4.30	0.602	0.670	1.79	1.10×10^{-8}
N719	13.96	0.783	0.713	7.89	–

4.2.3. Compound **3**

A mixture of porphyrin **2** (410 mg, 0.34 mmol) and NBS (0.14 g, 0.80 mmol) in DCM (250 mL) was stirred at 0 °C under argon for 3 h. The reaction was quenched with acetone (20 mL) and the solvent was removed under reduced pressure. The crude was purified by column chromatography (silica gel) using DCM:hexanes (1:1) as the eluant to give the product (380 mg, 87%) as a green solid, mp = 132 °C. ^{1}H NMR (600 MHz, $CDCl_3$) δ_H 0.38–0.67 (m, 44H), 0.78–0.83 (m, 8H), 0.93–0.98 (m, 8H), 3.81 (t, $J = 6.4$ Hz, 8H), 6.82 (t, $J = 7.3$ Hz, 2H), 6.95 (d, $J = 8.3$ Hz, 4H), 7.12 (t, $J = 9.2$ Hz, 4H), 7.31 (d, $J = 7.3$ Hz, 4H), 7.65 (t, $J = 8.3$ Hz, 2H), 8.74 (d, $J = 4.6$ Hz, 2H), 8.87 (d, $J = 4.6$ Hz, 2H), 9.19 (d, $J = 4.6$ Hz, 2H), 9.61 (d, $J = 4.6$ Hz, 2H) ppm; ^{13}C NMR (151 MHz, $CDCl_3$) δ_C 13.8, 22.2, 22.3, 25.1, 28.4, 28.5, 28.6, 29.8, 31.3, 31.4, 68.5, 104.0, 105.1, 114.2, 120.5, 120.6, 120.8, 122.1, 128.9, 129.9, 130.4, 132.4, 132.5, 132.8, 149.3, 150.2, 151.4, 152.1, 152.3, 152.5, 159.9 ppm; FT-IR (KBr) υ = 3034, 2950, 2925, 2852, 1586, 1492, 1458, 1438, 1370, 1262, 1242 cm^{-1}; MS (MALDI-TOF): *m/z* 1281.114. Anal. Calcd. for $C_{76}H_{92}BrN_5O_4Zn$: C, 71.14; H, 7.18; N, 5.46. Found: C, 71.21; H, 7.07; N, 5.48.

4.2.4. Compound **4**

A mixture of porphyrin **3** (323 mg, 0.25 mmol), 9,9-dioctyl-7-vinyl-9*H*-fluorene-2-carbaldehyde (223.5 mg, 0.50 mmol), $Pd(OAc)_2$ (5.6 mg, 0.025 mmol), tetra-butylammonium bromide (TBAB) (239.6, 0.75 mmol), potassium carbonate (K_2CO_3) (104.1 mg, 0.75 mmol) in 30 mL of DMF was heated at 110 °C under an inert atmosphere for 24 h. The reaction was quenched with 40 mL of water and extracted with $CHCl_3$ (3 × 50 mL). The organic phase was washed with water twice and dried over anhydrous magnesium sulfate ($MgSO_4$). The solvent was removed under vacuum. The crude was purified by column chromatography (silica gel) using DCM:hexanes (1:1) as the eluant to give the product (335 mg, 81%) as a green solid, mp = 97 °C. ^{1}H NMR (600 MHz, $CDCl_3$) δ_H 0.42–0.65 (m, 44H), 0.77–0.81 (m, 16H), 0.94–0.99 (m, 8H), 1.10–1.22 (m, 22H), 2.12 (t, $J = 7.3$ Hz, 4H), 3.81 (t, $J = 6.4$ Hz, 8H), 6.8 (t, $J = 7.3$ Hz, 2H), 6.95 (d, $J = 8.3$ Hz, 4H), 7.12 (t, $J = 9.2$ Hz, 4H), 7.33 (d, $J = 8.3$ Hz, 2H), 7.47 (d, $J = 15.6$ Hz, 1H), 7.64 (t, $J = 8.3$ Hz, 2H), 7.82 (s, 1H), 7.92–7.93 (m, 3H), 7.96 (d, $J = 7.3$ Hz, 1H), 8.00 (d, $J = 7.3$ Hz, 1H), 8.74 (d, $J = 4.6$ Hz, 2H), 8.89 (d, $J = 4.6$ Hz, 2H) 9.18 (d, $J = 4.6$ Hz, 2H), 9.52 (d, $J = 4.6$ Hz, 2H), 9.75 (d, $J = 16.5$ Hz, 1H), 10.10 (s, 1H) ppm; ^{13}C NMR (151 MHz, $CDCl_3$) δ_C 13.9, 14.2, 22.3, 22.7, 24.0, 25.1, 28.5, 28.6, 28.7, 29.4, 30.1, 30.2, 31.4, 31.9, 40.4, 40.5, 55.3, 55.5, 68.6, 85.0, 105.2, 113.7, 113.8, 120.1, 120.4, 121.1, 121.6, 122.1, 123.2, 124.2, 125.7, 128.9, 129.7, 129.8, 130.0, 130.1, 130.8, 130.9, 131.4, 132.5, 141.9, 149.2, 149.9, 150.7, 152.0, 152.1, 152.4, 160.0, 192.5 ppm; FT-IR (KBr) υ = 2953, 2924, 2852, 1693, 1592, 1456, 1379, 1246 cm^{-1}; MS (MALDI-TOF): *m/z* 1646.132. Anal. Calcd. for $C_{108}H_{135}N_5O_5Zn$: C, 78.74; H, 8.20; N, 4.25. Found: C, 78.61; H, 8.27; N, 4.32.

4.2.5. Dye **5a**

A mixture of compound **4** (84 mg, 0.051 mmol), cyanoacetic acid (130.1 mg, 1.53 mmol), and piperidine (0.5 mL) in absolute ethanol (25 mL) was EtOH was refluxed for 24 h. The reaction mixture was then cooled to room temperature and extracted with DCM. The organic phase was washed with water twice and dried over anhydrous $MgSO_4$. The solvent was removed under vacuum and the crude was purified by column chromatography (silica gel) using DCM:MeOH (20:1) as the eluant to give the product (62 mg, 72%) as a green solid, mp = 155 °C. ^{1}H NMR (600 MHz, DMSO-d_6) δ_H 0.34–0.66 (m, 32H), 0.71–0.82 (m, 22H), 0.85–0.96 (m, 18H),

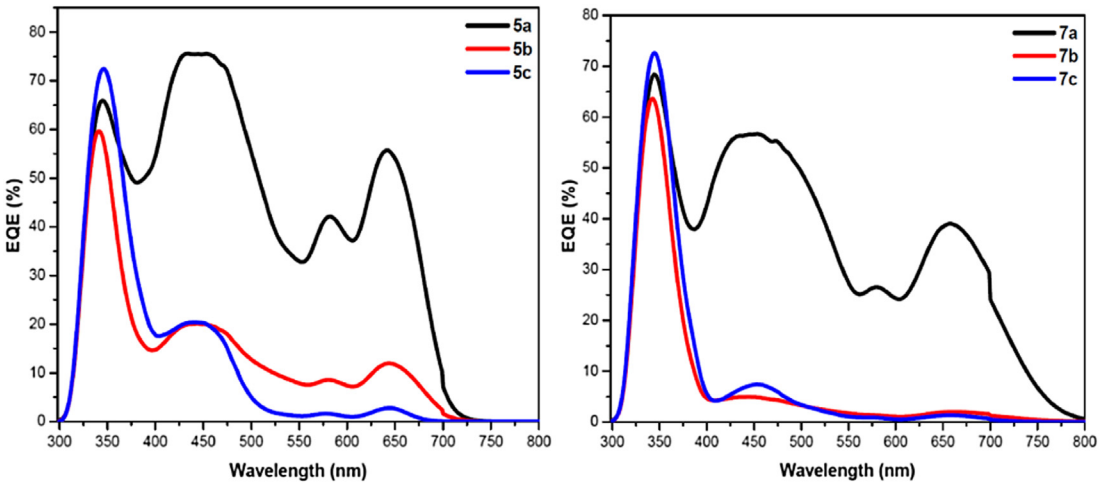

Fig. 7. EQE plots of devices based on dyes **5a**–**c** and **7a**–**c** for best EQE data. Devices were tested using a Bentham PVE300 photovoltaic characterization system.

1.07–1.15 (m, 18H), 2.14 (t, J = 7.3 Hz, 4H), 3.77–3.85 (m, 8H), 6.79 (t, J = 6.9 Hz, 2H), 7.04 (d, J = 9.2 Hz, 4H), 7.12 (t, J = 7.8 Hz, 4H), 7.21 (d, J = 8.25 Hz, 4H), 7.30 (d, J = 15.6 Hz, 1H), 7.65 (t, J = 8.7 Hz, 2H), 7.92 (d, J = 7.3 Hz, 1H), 7.97–8.06 (m, 6H), 8.50 (d, J = 4.6 Hz, 2H), 8.62 (d, J = 4.6 Hz, 2H), 8.95 (d, J = 4.6 Hz, 2H) 9.43 (d, J = 4.6 Hz, 2H), 9.86 (d, J = 15.6 Hz, 1H) ppm; ^{13}C NMR (151 MHz, $CDCl_3$) δ_C 14.0, 14.2, 22.2, 22.4, 22.7, 22.8, 23.5, 24.1, 25.2, 26.4, 28.5, 28.6, 28.7, 28.8, 29.4, 29.4, 29.7, 29.8, 30.2, 31.5, 31.9, 32.0, 32.3, 40.4, 55.5, 56.0, 68.5, 76.9, 77.1, 77.3, 105.0, 113.6, 116.3, 120.2, 120.4, 121.1, 121.4, 122.1, 125.1, 128.9, 129.7, 129.7, 130.0, 131.3, 131.4, 132.4, 135.3, 149.2, 149.8, 150.5, 151.8, 152.1, 152.5, 159.9 ppm; FT-IR (KBr) υ = 3421, 2957, 2928, 2855, 2216, 1718, 1595, 1464 1365, 1284, 1258 cm^{-1}; MS (MALDI-TOF): *m/z* 1713.903. Anal. Calcd. for $C_{111}H_{136}N_6O_6Zn$: C, 77.76; H, 7.94; N, 4.90. Found: C, 77.83; H, 7.90; N, 5.02.

4.2.6. Dye ***5b***

A mixture of compound **4** (88 mg, 0.053 mmol), 4-oxo-2-thioxo-3-thiazolidinylacetic acid (202 mg, 1.06 mmol), and ammonium acetate (81.67 mg, 1.06 mmol) in AcOH (25 mL) was refluxed for 30 h. The reaction mixture was then cooled to room temperature and extracted with DCM. The organic phase was washed with water twice and dried over anhydrous $MgSO_4$. The solvent was removed under vacuum and the crude was purified by column chromatography (silica gel) using DCM:MeOH (20:1) as the eluant to give the product (68 mg, 70%) as a green solid, mp = 170 °C. ^{1}H NMR (600 MHz, DMSO-d_6) δ_H 0.30–0.51 (m, 32H), 0.66–0.71 (m, 22H), 0.83–0.89 (m, 18H), 1.03–1.08 (m, 18H), 2.06–2.16 (m, 4H), 3.73–3.79 (m, 8H), 4.71 (br. s, 2H), 6.75 (t, J = 7.3 Hz, 2H), 6.99 (d, J = 9.2 Hz, 4H), 7.08 (t, J = 7.8 Hz, 4H), 7.17 (d, J = 8.3 Hz, 4H), 7.27 (d, J = 15.6 Hz, 1H), 7.60 (t, J = 8.7 Hz, 2H), 7.66 (d, J = 8.3 Hz, 1H), 7.71 (s, 1H), 7.95–7.96 (m, 2H), 8.02–8.06 (m, 3H), 8.46 (d, J = 4.6 Hz, 2H), 8.58 (d, J = 4.6 Hz, 2H), 8.92 (d, J = 4.6 Hz, 2H), 9.40 (d, J = 4.6 Hz, 2H), 9.85 (d, J = 16.5 Hz, 1H) ppm; ^{13}C NMR (151 MHz, $CDCl_3$) δ_C 13.9, 14.2, 22.3, 22.7, 24.1, 25.2, 28.5, 28.6, 28.7, 29.4, 29.8, 30.2, 31.4, 31.9, 40.5, 55.5, 68.7, 76.9, 77.1, 77.3, 105.3, 113.8, 116.9, 120.4, 120.7, 120.9, 121.1, 121.2, 121.3, 121.6, 122.1, 125.2, 126.0, 128.9, 129.7, 129.8, 130.1, 130.8, 130.9, 131.4, 131.9, 132.5, 135.3, 139.0, 139.6, 142.0, 144.4, 149.3, 149.9, 150.7, 152.1, 152.4, 152.8, 160.0 ppm; FT-IR (KBr) υ = 3423, 2956, 2924, 2854, 1713, 1595, 1460, 1360, 1282, 1259, cm^{-1}; MS (MALDI-TOF): *m/z* 1819.217. Anal. Calcd. for $C_{113}H_{138}N_6O_7S_2Zn$: C, 74.55; H, 7.59; N, 4.62. Found: C, 74.63; H, 7.65; N, 4.54.

4.2.7. Dye ***5c***

A mixture of compound **4** (80 mg, 0.049 mmol), 2-(1,1-dicyanomethylene)-1,3-thiazol-4-one (160 mg, 0.97 mmol), and piperidine (0.5 mL) in absolute ethanol (20 mL) was refluxed for 40 h. The reaction mixture was then cooled to room temperature and extracted with DCM. The organic phase was washed with water twice and dried over anhydrous $MgSO_4$. The solvent was removed under vacuum and the crude was purified by column chromatography (silica gel) using DCM:MeOH (30:1) as the eluent to give the product (66 mg, 75%) as a green solid, mp = 188 °C. ^{1}H NMR (600 MHz, DMSO-d_6) δ_H 0.34–0.63 (m, 32H), 0.72–0.90 (m, 40H), 1.07–1.14 (m, 18H), 2.14 (t, J = 7.3 Hz, 4H), 3.76–3.83 (m, 8H), 6.80 (t, J = 7.3 Hz, 2H), 7.03 (d, J = 9.2 Hz, 4H), 7.11 (t, J = 7.8 Hz, 4H), 7.21 (d, J = 8.3 Hz, 4H), 7.29 (d, J = 15.6 Hz, 1H), 7.64 (t, J = 8.7 Hz, 2H), 7.70 (d, J = 8.7 Hz, 2H), 7.91 (s, 1H), 7.96–8.07 (m, 4H), 8.49 (d, J = 4.6 Hz, 2H), 8.62 (d, J = 4.6 Hz, 2H), 8.95 (d, J = 4.6 Hz, 2H) 9.12 (br. s, 1H), 9.43 (d, J = 4.6 Hz, 2H), 9.86 (d, J = 15.6 Hz, 1H) ppm; ^{13}C NMR (151 MHz, $CDCl_3$) δ_C 13.9, 14.2, 22.3, 22.7, 22.8, 24.1, 24.8, 25.2, 25.8, 28.5, 28.6, 28.7, 29.2, 29.4, 29.5, 29.5, 29.7, 29.8, 30.2, 31.4, 31.9, 32.0, 34.1, 40.5, 50.2, 55.4, 55.9, 68.6, 105.3, 113.7, 120.4, 120.5, 120.9, 121.0, 121.3, 121.5, 122.1, 125.5, 125.9, 126.0, 128.0, 128.1, 128.9, 129.3, 129.8, 130.0, 130.1, 130.3, 131.3, 132.4, 133.1, 149.3, 149.9, 150.7, 152.1, 152.2, 152.5, 160.0, 161.2, 162.9, 179.5, 181.5, 183.4 ppm; FT-IR (KBr) υ = 3343, 2955, 2925, 2854, 2210, 1720, 1595, 1462, 1367, 1284, 1257 cm^{-1}; MS (MALDI-TOF): *m/z* 1793.355. Anal. Calcd. for $C_{114}H_{136}N_8O_5SZn$: C, 76.30; H, 7.58; N, 6.25. Found: C, 76.37; H, 7.49; N, 6.31.

4.2.8. Compound ***6***

A mixture of porphyrin **3** (420 mg, 0.33 mmol), 5-vinylthiophene-2-carbaldehyde (90.2 mg, 0.65 mmol), $Pd(OAc)_2$ (7.3 mg, 0.033 mmol), TBAB (311.6, 0.98 mmol), and K_2CO_3 (135.4 mg, 0.98 mmol) in DMF (30 mL) was heated at 110 °C under an inert atmosphere for 48 h. The reaction was then quenched with water (40 mL) and extracted with $CHCl_3$ (3 × 60 mL). The combined organic extracts were dried over anhydrous $MgSO_4$ and the solvent was removed under vacuum. The crude was purified by column chromatography (silica gel) using DCM:hexanes (2:1) as the eluent to give the product (280 mg, 64%) as a green solid, mp = 108 °C. ^{1}H NMR (600 MHz, $CDCl_3$) δ_H 0.39–0.66 (m, 44H), 0.75–0.80 (m, 8H), 0.93–0.98 (m, 8H), 3.81 (t, J = 6.4 Hz, 8H), 6.82 (t, J = 7.3 Hz, 2H), 6.95 (d, J = 8.3 Hz, 4H), 7.12 (t, J = 7.8 Hz, 4H), 7.31 (d, J = 9.2 Hz, 4H), 7.41 (d, J = 3.7 Hz, 1H), 7.49 (d, J = 15.6 Hz, 1H), 7.65 (t, J = 8.7 Hz,

2H), 7.84 (d, J = 3.7 Hz, 1H), 8.72 (d, J = 4.6 Hz, 2H), 8.89 (d, J = 4.6 Hz, 2H), 9.18 (d, J = 4.6 Hz, 2H), 9.43 (d, J = 4.6 Hz, 2H), 9.76 (d, J = 15.6 Hz, 1H), 10.00 (s, 1H) ppm; ^{13}C NMR (151 MHz, $CDCl_3$) δ_C 13.9, 22.3, 25.2, 28.5, 28.6, 28.7, 29.8, 31.4, 68.6, 105.2, 114.3, 114.6, 120.5, 120.9, 121.8, 122.2, 126.9, 129.0, 129.2, 129.9, 130.3, 131.9, 132.6, 133.0, 135.2, 137.6, 141.6, 149.0, 150.1, 150.7, 152.1, 152.4, 153.1, 159.9, 182.6, 183.0 ppm; FT-IR (KBr) υ = 2954, 2924, 2853, 1722, 1591, 1461, 1376, 1259 cm^{-1}; MS (MALDI-TOF): m/z 1340.104. Anal. Calcd. for $C_{83}H_{97}N_5O_5SZn$: C, 74.33; H, 7.24; N, 5.22. Found: C, 74.49; H, 7.34; N, 4.95.

4.2.9. Dye **7a**

A mixture of compound **6** (40 mg, 0.029 mmol), cyanoacetic acid (50.7 mg, 0.59 mmol), and piperidine (0.4 mL) in absolute ethanol (20 mL) was refluxed for 20 h. The reaction mixture was then cooled to room temperature and extracted with DCM. The organic phase was washed with water twice and dried over anhydrous $MgSO_4$. The solvent was removed under vacuum and the crude was purified by column chromatography (silica gel) using DCM:MeOH (20:1) as the eluent to give the product (29 mg, 70%) as a green solid, mp = 167 °C. ^{1}H NMR (600 MHz, DMSO-d_6) δ_H 0.33–0.62 (m, 30H), 0.70–0.89 (m, 30H), 3.80 (t, J = 6.0 Hz, 8H), 6.78 (t, J = 7.3 Hz, 2H), 7.04 (d, J = 8.3 Hz, 4H), 7.11 (t, J = 7.8 Hz, 4H), 7.20 (d, J = 8.3 Hz, 4H), 7.40 (d, J = 15.6 Hz, 1H), 7.63–7.66 (m, 3H), 7.79 (br. s, 1H), 8.15 (br. s, 1H), 8.48 (d, J = 4.6 Hz, 2H), 8.62 (d, J = 4.6 Hz, 2H), 8.94 (d, J = 3.7 Hz, 2H), 9.36 (d, J = 4.6 Hz, 1H), 9.64 (d, J = 14.7 Hz, 1H) ppm; ^{13}C NMR (151 MHz, $CDCl_3$) δ_C 13.8, 14.1, 22.2, 22.6, 22.7, 25.1, 28.5, 28.6, 29.8, 31.3, 51.9, 53.4, 53.6, 55.9, 68.6, 105.2, 105.3, 114.1, 114.2, 120.4, 122.1, 128.9, 129.7, 130.0, 131.7, 132.4, 149.1, 150.0, 150.7, 152.0, 152.5, 159.9 ppm; FT-IR (KBr) υ = 3428, 2953, 2218, 1721, 1587, 1367, 1456, 1383, 1248 cm^{-1}; MS (MALDI-TOF): m/z 1407.737. Anal. Calcd. for $C_{86}H_{98}N_6O_6SZn$: C, 73.35; H, 6.97; N, 5.97. Found: C, 73.31; H, 6.99; N, 5.93.

4.2.10. Dye **7b**

A mixture of compound **6** (60 mg, 0.045 mmol), 4-oxo-2-thioxo-3-thiazolidinylacetic acid (170 mg, 0.89 mmol), ammonium acetate (68.95 mg, 0.89 mmol) in AcOH (20 mL) was refluxed for 30 h. The reaction mixture was then cooled to room temperature and extracted with DCM. The organic phase was washed with water twice and dried over anhydrous $MgSO_4$. The solvent was removed under vacuum and the crude was purified by column chromatography (silica gel) using DCM:MeOH (20:1) as the eluent to give the product (44 mg, 65%) as a green solid, mp = 182 °C. ^{1}H NMR (600 MHz, DMSO-d_6) δ_H 0.34–0.67 (m, 30H), 0.72–0.92 (m, 30H), 3.81 (t, J = 6.0 Hz, 8H), 5.3 (br. s, 2H), 6.80 (t, J = 7.3 Hz, 2H), 7.04 (d, J = 8.2 Hz, 4H), 7.16 (t, J = 7.8 Hz, 4H), 7.27 (d, J = 8.3 Hz, 4H), 7.47 (d, J = 15.8 Hz, 1H), 7.66 (t, J = 8.9 Hz, 2H), 7.75 (br. s, 1H), 7.90 (br. s, 1H), 8.18 (br. s, 1H), 8.50 (d, J = 4.8 Hz, 2H), 8.62 (d, J = 4.1 Hz, 2H), 8.93 (d, J = 4.1 Hz, 2H), 9.42 (d, J = 4.1 Hz, 2H), 9.77 (d, J = 15.8 Hz, 1H) ppm; ^{13}C NMR (151 MHz, $CDCl_3$) δ_C 13.8, 14.1, 22.2, 22.7, 25.1, 28.5, 28.6, 29.4, 29.6, 29.7, 31.3, 48.3, 52.1, 53.2, 56.0, 68.6, 76.8, 77.1, 77.3, 105.2, 114.3, 120.4, 122.1, 122.6, 128.9, 129.1, 129.8, 131.8, 132.5, 132.6, 149.1, 150.0, 150.7, 151.7, 153.5, 159.9 ppm; FT-IR (KBr) υ = 3412, 2956, 2925, 2853, 1731, 1591, 1459, 1389, 1356, 1256, cm^{-1}; MS (MALDI-TOF): m/z 1513.574. Anal. Calcd. for $C_{88}H_{100}N_6O_7S_3Zn$: C, 69.79; H, 6.61; N, 5.55. Found: C, 69.84; H, 6.49; N, 5.61.

4.2.11. Dye **7c**

A mixture of compound **6** (40 mg, 0.029 mmol), 2-(1,1-dicyanomethylene)-1,3-thiazol-4-one (98.3 mg, 0.59 mmol), and piperidine (0.4 mL) in absolute ethanol (20 mL) was refluxed for 20 h. The reaction mixture was then cooled to room temperature and extracted with DCM. The organic phase was washed with water twice and dried over anhydrous $MgSO_4$. The solvent was removed under vacuum and the crude was purified by column chromatography (silica gel) using DCM:MeOH (30:1) as the eluent to give the product (30 mg, 68%) as a green solid, mp = 195 °C. ^{1}H NMR (600 MHz, DMSO-d_6) δ_H 0.31–0.65 (m, 30H), 0.71–0.91 (m, 30H), 3.80 (t, J = 5.5 Hz, 8H), 6.79 (t, J = 7.3 Hz, 2H), 7.04 (d, J = 9.2 Hz, 4H), 7.11 (t, J = 7.3 Hz, 4H), 7.20 (d, J = 8.3 Hz, 4H), 7.42 (d, J = 15.6 Hz, 1H), 7.63–7.67 (m, 3H), 7.86 (s, 1H), 7.91 (s, 1H), 8.48 (d, J = 4.6 Hz, 2H), 8.61 (d, J = 4.6 Hz, 2H), 8.94 (d, J = 4.6 Hz, 2H), 9.10 (br. s, 1H), 9.37 (d, J = 4.6 Hz, 2H), 9.64 (d, J = 16.5 Hz, 1H) ppm; ^{13}C NMR (151 MHz, $CDCl_3$) δ_C 13.8, 14.1, 22.3, 22.4, 22.6, 22.7, 24.0, 24.8, 24.9, 25.1, 25.8, 26.6, 26.7, 27.3, 28.5, 28.6, 28.8, 29.1, 29.2, 29.3, 29.4, 29.5, 29.6, 29.7, 29.8, 29.9, 31.4, 32.0, 33.8, 33.9, 40.7, 46.9, 50.0, 50.1, 50.2, 53.4, 53.5, 55.9, 56.0, 68.7, 105.3, 105.4, 120.4, 121.3, 122.0, 122.1, 128.9, 129.4, 129.6, 129.7, 129.8, 129.9, 130.0, 131.6, 132.4, 149.1, 150.0, 150.7, 152.0, 152.4, 152.5, 159.9, 160.0, 162.8, 163.1, 177.7 ppm; FT-IR (KBr) υ = 3359, 2952, 2925, 2853, 2213, 1722, 1590, 1460, 1368, 1253, cm^{-1}; MS (MALDI-TOF): m/z 1487.644. Anal. Calcd. for $C_{89}H_{98}N_8O_5S_2Zn$: C, 71.82; H, 6.59; N, 7.53. Found: C, 71.79; H, 6.39; N, 7.64.

4.3. Electrochemical and solar cell measurements

All electrochemical measurements were recorded using a conventional three-electrode configuration consisting of a glassy carbon working electrode, a silver wire as a pseudo-reference electrode, and a platinum wire as the auxiliary electrode at a scan rate of 100 mV/s at room temperature. Samples were first degassed with a gentle flow of argon for 5 min prior to the scans. The potentials were calibrated relative to the Fc/Fc + couple.

A 20 nm TiO_2 paste was synthesized from Sigma–Aldrich Aeroxide TiO_2 powder by a previously reported sol gel method [26]. An electrolyte solution of 0.6 M DMPII, 0.03 M I_2, 0.1 M guanidinium thiocyanate, and 0.50 M 4-tert-butylpyridine in acetonitrile was used for the dye studies. The Pt counterelectrodes were manufactured from FTO (2 cm by 2 cm) cleaned in a 0.1 M HCl solution in ethanol, and then sonicated in acetone for 10 min. Substrates were then dried at 400 °C for 15 min and cooled. Upon cooling, a drop of H_2PtCl_6 in ethanol (2 mg Pt in 1 mL EtOH) was placed on each substrate and then the substrates were sintered at 400 °C for 15 min.

FTO was purchased from Sigma–Aldrich in 300 mm by 300 mm sheets at 7Ω/square and were cut to 2 cm by 2 cm. Literature procedures were followed for device manufacturing but is also reported here [27]. The sized FTO was then sonicated in a 2% Alconox detergent solution for 20 min, rinsed and then sonicated in ethanol for 20 min. Cells were then dried and UV treated for 18 min in a Jelight Company Model 342 UV-Ozone apparatus. Clean FTO was then treated with a 40 mM aqueous solution of $TiCl_4$ for 30 min at 70 °C, rinsed with diH_2O and ethanol, and then doctor-bladed with the TiO_2 paste. The TiO_2 layer was then heated at 325 °C for 5 min, 375 °C for 5 min, 450 °C for 15 min, and finally 500 °C for 15 min and allowed to cool. This was done twice and then a final $TiCl_4$ layer was applied following the same conditions, once dried, they were heated at 500 °C for 30 min. After cooling, a TiO_2 electrode was immersed in 0.3 mM of each respective dye. Cyanoacrylic acid dye electrodes (**5a**, **7a**) were removed after 20 h, rhodanine acid dye electrodes (**5b**, **5c**) were removed after 12 h, and dicyano rhodanine electrodes (**5c**, **7c**) were removed after 24 h of soaking. After making electrodes approximately 0.25 cm^2 in area a tape gasket was used and electrolyte was loaded into the cell and backed with a Pt counter electrode. All cells were tested using

a Photo Emission Tech SS100 Solar Simulator at approximately 100 mW/cm^2.

4.4. Computational methods

All the new structures and the geometric and electronic properties were optimized using the GAUSSIAN-09 package at the density functional theory (DFT) level. M06 was the meta-hybrid functional employed, which includes the last dispersion approximation performed by Truhlar. The basis set chosen for all the atoms was the Pople 6-31G**.

Acknowledgments

The authors gratefully acknowledge financial support from COLCIENCIAS, the Universidad del Valle, project PRI-PRIBUS-2011-1067, the Robert A. Welch Foundation for an endowed chair (Grant #AH-0033), the U.S. Air Force grants AFOSR-FA9550-12-1-0053 and AFOSR-FA9550-12-1-0468, MINECO of Spain (Projects CTQ2011-24652, Consolider-Ingenio 2010C-07–25200) and CAM (MADRI-SOLAR Project P-PPQ-000225-0505).

Appendix A. Supplementary data

Supplementary data related to this article can be found at http://dx.doi.org/10.1016/j.dyepig.2014.06.028.

References

[1] Grätzel M. Photoelectrochemical cells. Nature 2001;414:338–44.
[2] Hagfeldt A, Boschloo G, Sun LC, Kloo L, Pettersson H. Dye sensitized solar cells. Chem Rev 2010;110:6595–663.
[3] a Nazeeruddin MK, Splivallo R, Liska P, Comte P, Grätzel M. A swift dye uptake procedure for dye sensitized solar cells. Chem Commun 2003;103:1456–7;
b Grätzel M. Conversion of sunlight to electric power by nanocrystalline dye-sensitized solar cells. J Photochem Photobiol A 2004;164:3–14;
c Wang P, Wenger B, Humphry-Baker R, Moser JE, Teuscher J, Kantlehner W, et al. Charge separation and efficient light energy conversion in sensitized mesoscopic solar cells based on binary ionic liquids. J Am Chem Soc 2005;127:6850–6;
d Wang P, Zakeeruddin SM, Exnar I, Grätzel M. High efficiency dye-sensitized nanocrystalline solar cells based on ionic liquid polymer gel electrolyte. Chem Commun 2002;24:2972–3.
[4] Tian H, Meng F. In: Sun S-S, Sariciftci NS, editors. Organic photovoltaics: mechanisms, materials and devices. London: CRC; 2005. pp. 313–4.
[5] a Loi MA, Denk P, Hoppe H, Neugebauer H, Winder C, Meissner D, et al. Long-lived photoinduced charge separation for solar cell applications in phthalocyanine–fulleropyrrolidine dyad thin films. J Mater Chem 2003;13:700–4;
b Wong MS, Li ZH, Tao Y, D'Iorio M. Synthesis and functional properties of donor–acceptor π-conjugated oligomers. Chem Mater 2003;15:1198–203;
c Jiao GS, Thoresen LH, Burgess K. Fluorescent, through-bond energy transfer cassettes for labeling multiple biological molecules in one experiment. J Am Chem Soc 2003;125:14668–9;
d Martín M, Sánchez L, Herranz MA, Illescas B, Guldi DM. Electronic communication in tetrathiafulvalene (TTF)/C_{60} systems: toward molecular solar energy conversion materials? Acc Chem Res 2007;40:1015–24;
e Wenger S, Bouit P-A, Chen Q, Teuscher J, Di Censo D, Humphry-Baker R, et al. Efficient electron transfer and sensitizer regeneration in stable π-extended tetrathiafulvalene-sensitized solar cells. J Am Chem Soc 2010;132:5164–9.
[6] a Kang SH, Choi IT, Kang MS, Eom YK, Ju MJ, Hong JY, et al. Novel D–π–A structured porphyrin dyes with diphenylamine derived electron-donating substituents for highly efficient dye-sensitized solar cells. J Mater Chem A 2013;1:3977–82;
b Yella A, Lee H-W, Tsao HN, Yi C, Chandiran AK, Nazeeruddin MK, et al. Porphyrin-sensitized solar cells with cobalt (II/III)–based redox electrolyte exceed 12 percent efficiency. Science 2011;334:629–33;
c Imahori H, Umeyama T, Ito S. Large π-aromatic molecules as potential sensitizers for highly efficient dye-sensitized solar cells. Acc Chem Res 2009;42:1809–18;
d Rochford J, Chu D, Hagfeldt A, Galoppini E. Tetrachelate porphyrin chromophores for metal oxide semiconductor sensitization: effect of the spacer length and anchoring group position. J Am Chem Soc 2007;129:4655–65;
e Campbell WM, Jolley KW, Wagner P, Wagner K, Walsh PJ, Gordon KC, et al. Highly efficient porphyrin sensitizers for dye-sensitized solar cells. J Phys Chem C 2007;111:11760–2;
f Imahori H, Umeyama T, Kurotobi K, Takano Y. Self-assembling porphyrins and phthalocyanines for photoinduced charge separation and charge transport. Chem Commun 2012;48:4032–45;
g Griffith MJ, Sunahara K, Wagner P, Wagner K, Wallace G, Officer DL, et al. Porphyrins for dye-sensitised solar cells: new insights into efficiency-determining electron transfer steps. Chem Commun 2012;48:4145–62;
h Rangan S, Katallinic S, Thorpe R, Bartynski RA, Rochford J, Galoppini E. Energy level alignment of a zinc (II) tetraphenylporphyrin dye adsorbed onto TiO_2 and ZnO surfaces. J Phys Chem C 2010;114:1139–47;
i KC C, Stranius K, D'Souza P, Subbaiyan NK, Lemmetyinen H, Tkachenko NV, et al. Sequential photoinduced energy and electron transfer directed improved performance of the supramolecular solar cell of a zinc porphyrin–zinc phthalocyanine conjugate modified TiO_2 surface. J Phys Chem C 2013;117:763–73;
j Rochford J, Galoppini E. Zinc (II) tetraarylporphyrins anchored to TiO_2, ZnO, and ZrO_2 nanoparticle films through rigid-rod linkers. Langmuir 2008;24:5366–74.
[7] Giribabu L, Sudhakar K, Velkannan V. Phthalocyanines: potential alternative sensitizers to Ru(II) polypyridyl complexes for dye-sensitized solar cells. Curr Sci India 2012;102:991–1000.
[8] a Tae EL, Lee SH, Lee JK, Yoo SS, Kang EJ, Yoon KB. A strategy to increase the efficiency of the dye-sensitized TiO_2 solar cells operated by photoexcitation of dye-to-TiO_2 charge-transfer bands. J Phys Chem B. 2005;109:22513–22;
b Dai Q, Rabani J. Photosensitization of nanocrystalline TiO_2 films by pomegranate pigments with unusually high efficiency in aqueous medium. Chem Commun 2001:2142–3;
c Dai Q, Rabani J. Unusually efficient photosensitization of nanocrystalline TiO_2 films by pomegranate pigments in aqueous medium. New J Chem 2002;26:421–6;
d Garcia CG, Polo AS, Iha NY. Fruit extracts and ruthenium polypyridinic dyes for sensitization of TiO_2 in photoelectrochemical solar cells. J Photochem Photobiol A 2003;160:87–91.
[9] Chauhan R, Trivedi M, Bahadur L, Kumar A. Application of π-extended ferrocene with varied anchoring groups as photosensitizers in TiO_2-based dye-sensitized solar cells (DSSCs). Chem Asian J 2011;6:1525–32.
[10] a Bruneti FG, López JL, Atienza C, Martín N. π-Extended TTF: a versatile molecule for organic electronics. J Mater Chem 2012;22:4188–205;
b Bouit P-A, Villegas C, Delgado JL, Viruela PM, Pou-Amerigo R, Ortí E, et al. ExTTF-based dyes absorbing over the whole visible spectrum. Org Lett 2011;13(4):604–7.
[11] a Xu W, Peng B, Chen J, Liang M, Cai F. New triphenylamine-based dyes for dye-sensitized solar cells. J Phys Chem C 2008;112:874–80;
b Chittratan P, Thanakit P, Jarernboon W, Phromyothin D. Efficiency improvement of triphenylamine-based organic dyes in DSSCs, an effects of linker moiety. Adv Mater Res 2013;802:257–61.
[12] Zhang S, Yang X, Numata Y, Han L. Highly efficient dye-sensitized solar cells: progress and future challenges. Energy Environ Sci 2013;6:1443–64.
[13] Numata Y, Islam A, Shirai Y, Han L. Preparation of donor–acceptor type organic dyes bearing various electron-withdrawing groups for dye-sensitized solar cell application. Chem Commun 2011;47:6159–61.
[14] a Horiuchi T, Miura H, Sumioka K, Uchida S. High efficiency of dye-sensitized solar cells based on metal-free indoline dyes. J Am Chem Soc 2004;126:12218–9;
b Yanga CH, Chen HL, Chuang YY, Wu CW, Chen CP, Liao SH, et al. Characteristics of triphenylamine-based dyes with multiple acceptors in application of dye-sensitized solar cells. J Power Sources 2009;188:627–34;
c Mao J, He N, Ning Z, Zhang Q, Guo F, Chen L, et al. Stable dyes containing double acceptors without COOH as anchors for highly efficient dye-sensitized solar cells. Angew Chem Int Ed 2012;51:9873–6.
[15] Ooyama Y, Inoue S, Nagano T, Kushimoto K, Ohshita J, Imae I, et al. Dye-sensitized solar cells based on donor–acceptor π-conjugated fluorescent dyes with a pyridine ring as an electron-withdrawing anchoring group. Angew Chem Int
Ed 2011;50:7429–33.
[16] a Lai H, Hong J, Liu P, Yuan C, Li Y, Fang Q. Multi-carbazole derivatives: new dyes for highly efficient dye-sensitized solar cells. RSC Adv 2012;2:2427–32;
b Panthi K, Adhikari RM, Kinstle TH. Carbazole donor–carbazole linker-based compounds: preparation, photophysical properties, and formation of fluorescent nanoparticles. J Phys Chem A 2010;114:4550–7.
[17] a Zhou H, Xue P, Zhang Y, Zhao X, Jia J, Zhang X. Fluorenylvinylenes bridged triphenylamine-based dyes with enhanced performance in dye-sensitized solar cells. Tetrahedron 2011;67:8477–83;
b Baheti A, Tyagi P, Justin Thomas KR, Hsu Y-C, T'suen Lin J. Simple triarylamine-based dyes containing fluorene and biphenyl linkers for efficient dye-sensitized solar cells. J Phys Chem C 2009;113:8541–7;
c Kim S-M, Balanay MP, Lee SH, Kim DH. Molecular engineering of fluorene-based photosensitizers for dye-sensitized solar cells. Bull Korean Chem Soc 2013;34(5):1329–30;
d Li W, Wu Y, Li X, Xie Y, Zhu W. Absorption and photovoltaic properties of organic solar cell sensitizers containing fluorene unit as conjunction bridge. Energy Environ Sci 2011;4:1830–7.
[18] Heredia D, Natera J, Gervaldo M, Otero L, Fungo F, Lin C-Y, et al. Spirobifluorene-bridged donor/acceptor dye for organic dye-sensitized solar cells. Org Lett 2010;12(1):12–5.

[19] a Feng Q, Zhang Q, Lu X, Wang H, Zhou G, Wang Z-S. A facile and selective synthesis of oligothiophene-based sensitizer isomers: an approach towards efficient dye-sensitized solar cells. Appl Mater Interfaces 2013;5(18):8982–90;
b Liu J, Li R, Si X, Zhou D, Shi Y, Wang Y. Oligothiophene dye-sensitized solar cells. Energy Environ Sci 2010;3:1924–8;
c Mishra A, Fischer MK, Bäuerle P. Metal-free organic dyes for dye-sensitized solar cells: from structure: property relationships to design rules. Angew Chem Int Ed 2009;48:2474–99.

[20] a Kwon T-H, Armel V, Nattestad A, MacFarlane DR, Bach U, Lind SJ, et al. Dithienothiophene (DTT)-Based dyes for dye-sensitized solar cells: synthesis of 2,6-Dibromo-DTT. J Org Chem 2011;76:4088–93;
b Qin H, Wenger S, Xu M, Gao F, Jing X, Wang P, et al. An organic sensitizer with a fused dithienothiophene unit for efficient and stable dye-sensitized solar cells. J Am Chem Soc 2008;130:9202–3.

[21] Insuasty A, Ortiz A, Tigreros A, Solarte E, Insuasty B, Martín N. 2-(1,1-dicyanomethylene)rhodanine: a novel, efficient electron acceptor. Dyes Pigment 2011;88:385–90.

[22] Williams A, Winfields S. Relative fluorescence quantum yields using a computer-controlled luminescence spectrometer. Analyst 1983;108:1067–71.

[23] Wang P, Zakeeruddin SM, Moser JE, Grätzel M. A new ionic liquid electrolyte enhances the conversion efficiency of dye-sensitized solar cells. J Phys Chem B. 2003;107:13280–5.

[24] Frisch MJ, Trucks GW, Schlegel HB, Scuseria GE, Robb MA, Cheeseman JR, et al. Gaussian 09, revision C.02. Wallingford CT: Gaussian, Inc.; 2009.

[25] Zhao Y, Truhlar D. The M06 suite of density functionals for main group thermochemistry, thermochemical kinetics, noncovalent interactions, excited states, and transition elements: two new functionals and systematic testing of four M06-class functionals and 12 other functionals. Theor Chem Acc 2008;120:215–41.

[26] Kim B, Chung K, Kim J. Molecular design principle of all-organic dyes for dye-sensitized solar cells. Chem Eur J 2013;19:5220–30.

[27] Ito S, Chen P, Comte P, Nazeeruddin M, Liska P, Péchy P, et al. Fabrication of screen-printing pastes from TiO_2 powders for dye-sensitized solar cells. Prog Photovolt Res Appl 2007;15:603–12.